ChemPhysChem

Research Article
doi.org/10.1002/cphc.202200454

Chemistry Europe
European Chemical Societies Publishing

www.chemphyschem.org

Effect of Nanoscale Confinement on Ultrafast Dynamics of Singlet Fission in TIPS-Pentacene

Yogita Silori,[a, b] Sakshi Chawla,[a] Anita Yadav,[a] and Arijit K. De*[a]

This work is dedicated to Prof. N. Sathyamurthy on 71.

Singlet fission (SF) is a phenomenon for the generation of a pair of triplet excitons from anexcited molecule in singlet electronic state interacting with another adjacent molecule in its ground electronic state. By increasing the effective number of charge carriers and reducing thermal dissipation of excess energy, SF is promised to enhance light-harvesting efficiency for photovoltaic applications. While SF has been extensively studied in thin films and crystals, the same has not been explored much within a confined medium. Here, we report the ultrafast SF dynamics of triisopropylsilylethynyl pentacene (TIPS-Pn) in micellar nanocavity of varying sizes (prepared from TX-100, CTAB, and SDS surfactants). The nanoparticles with a smaller size contain weakly coupled chromophores which are shown to be more efficient for SF followed by triplet generation as compared to the nanoparticles of larger size which contain strongly coupled chromophores which are less efficient due to the presence of singlet exciton traps. Through these studies, we delineate how a subtle interplay between short-range and long-range interaction among chromophores confined within nanoparticles, fine-tuned by the curvature of the micellar interface but irrespective of the nature of the micelle (cationic or anionic or neutral), play a crucial role in SF through and generation of triplets.

Introduction

Unravelling the mechanism of energy transfer leading to generation, separation, and recombination of charges (electron-hole pairs, known as Frenkel excitons) in artificial molecular systems has been a fascinating area of research. The model systems that mimic photosynthetic antenna can be described as molecular aggregates in which molecular excitonic energy levels depend on the relative arrangement of transition dipoles of monomers. Kasha introduced the terminology J- and H-aggregates for the head-to-tail arrangement and co-facial stacks, respectively, of the molecules coupled through space,[1–4] and such aggregates have been extensively used in optoelectronic devices at nanoscale dimensions. The thermal dissipation of excess energy (following absorption of high energy photons) by semiconductor materials, is one of the major reasons behind the limited efficiency of charge transfer within single-junction solar cells only up to 33%, known as the Shockley-Queisser limit.[5] Therefore, the focus of research has been moved to designing organic materials that can generate multiple excitons using high energy photons, and such process is known as singlet fission (SF) where the singlet excited molecule interacts with the adjacent ground state molecule to generate triplet excited states of both (^{1}TT). In order to satisfy the condition for efficient SF, energy of singlet excited state [E (^{1}S)] must be greater (or at least equal) to the energy of two triplet states [2E (^{1}T)].[6–10] The generated triplet excitons are quite long-lived which makes them perfect candidates for photovoltaic materials. However, only a few chromophores like acenes,[11–15] perylene diimide,[16–18] polyenes,[19–21] 1, 3-diphenylisobenzofuran,[22–23] etc can meet the condition discussed above. Previously, triplet excitonic dynamics in polyacenes (tetracene, pentacene and their derivatives), carotenoids, etc were explored using femtosecond to nanosecond transient absorption spectroscopy (TAS).[24–27] Two-dimensional electronic spectroscopy (2DES) was also employed to reveal electronic and vibrational coupling dynamics which are responsible for the coupling of bright ^{1}S and dark ^{1}TT excitons (electronically coupled triplet pair state which is also known as a multi-excitonic state) in thin film of pentacene derivatives.[28] The through-bond coupling (covalent linkage) between chromophore pairs (by using a variety of linkers) was found to be more prominent than the through-space coupling, which further enhances with an increase in conjugation.[29] Coherent[30–33] or incoherent[32–33] type of mechanism was identified during SF either due to superposition or population migration among ^{1}S and (^{1}TT) states. Tetracene and pentacene derivatives are used extensively to study the role of excimer in triplet-triplet annihilation and SF dynamics in nanoparticles (NPs).[34–40] Studies on SF dynamics in NPs of pentacene derivatives showed that the generation of triplet pair is mainly dependent on molecular packing inside the nanocavities which, in turn, fine-tunes the intermolecular coupling. Broadly, such coupling can be categorized in two types: type I having little long-range order and type II exhibiting extensive long-range (solid-state)

[a] Y. Silori, S. Chawla, A. Yadav, A. K. De
Condensed Phase Dynamics Group, Department of Chemical Sciences, Indian Institute of Science Education and Research (IISER) Mohali
Knowledge City, Sector 81, SAS Nagar, Punjab 140 306, India
E-mail: akde@iisermohali.ac.in

[b] Y. Silori
Present affiliation: Department of Physics, University of Michigan
Ann Arbor, Michigan 48109, United States

Supporting information for this article is available on the WWW under https://doi.org/10.1002/cphc.202200454

order. Strong intermolecular coupling (type II) resulting from brickwork packing motif leads to rapid SF as compared to weak coupling (type I), resulting from linear arrangement, a terminology we follow here from previous report.[35] In addition to the coupling strength, morphological evolution of NPs may also affect the packing into a polymorph significantly which may further affect the efficiency of singlet fission.[36,41–46] Such types of molecular packing arrangements have been studied using *ab initio* and semiempirical electronic structure calculations for various chromophores.[41–46] Using a constrained density functional theory including configuration interaction (CDFT-CI), the coupling strengths and fission rates of TIPS-Pn in solid-state 2D π-stacks were estimated[45] by considering the crystals as a valid structural model for dimer pairs in the poly- and nanocrystalline thin films[47] which were found to be responsible for line broadening and spectral redshift. However, in TIPS-Pn nanoparticles, a nonzero positional displacement along short-axis with a significant displacement along long-axis (slipped-stacked configurations) are observed within pairs[35,44] which ultimately lead to a bricklayer packing motif. It was shown that the strong intermolecular coupling can generate singlet exciton traps, resulting in less triplet generation and hence with lower SF efficiency.[36] Recently, it has been shown that the SF dynamics of TIPS-Pn in PMMA NPs become slower with no change in the dissociation rate of correlated triplets (^{1}TT); however, the triplet pair decays faster with an increase in concentration of PMMA.[48] These studies hint that the nanoparticle size-dependent interchromophoric couplings can affect the rate of SF and further our understanding of the mechanism of SF.

In this article, extending preliminary studies communicated elsewhere,[49] we present the role of confinement on the mechanism of SF of bis (triisopropylsilylethynyl) pentacene (TIPS-Pn) within nanosized TX-100 (neutral), CTAB (cationic), and SDS (anionic) micellar confinements. Time-resolved fluorescence lifetime and anisotropy reveal the presence of singlet excitonic energy migration within strongly coupled chromophores (type II) within NPs which significantly increase with size. From global analysis of femtosecond transient absorption data, we show that an increase in the size of the micellar NP, irrespective of the nature of headgroup (cationic, anionic or neutral), leads to the strong coupling between TIPS-Pn molecules which can give rise to singlet excitonic energy traps. Due to such energy traps, the rates of SF followed by triplet generation can be significantly reduced.

Experimental

Materials

6,13-bis(triisopropylsilylethynyl) pentacene (TIPS-Pn) (HPLC, $\geq$99%), sodium dodecyl sulfate (SDS) (ACS reagent, $\geq$99%), hexadecyltrimethylammonium bromide (CTAB) ($\geq$98%), t-octylphenoxypolyethoxyethanol (TX-100) (laboratory grade) and chloroform ($CHCl_3$) (HPLC, $\geq$99.9%) are purchased from Sigma Aldrich and used without any further purification. To prepare micellar solutions deionized water (Ultrapure, Merck Inc) is used.

NP Preparation and Characterization

A stock solution of TIPS-Pn with concentration $\sim 0.91 \times 10^3 M$ ($\varepsilon = 3.3 \times 10^4 M^{-1} cm^{-1}$ at 640 nm[50]) is prepared in $CHCl_3$ with optical density $\sim$3 using a 1 mm quartz absorption cell (Hellma Analytics). The stock solutions of TX-100, CTAB, and SDS surfactants are prepared in deionized water with concentrations $\sim$10 mM, 0.95 mM, and 8.2 mM, respectively, which are above their CMCs. For preparation of different NPs, 200/400/600/800/1000 μL of stock solution is injected into the 2 ml of surfactant solution with a continuous vigorous stirring for up to 2–3 hours and then kept for stabilization over a few minutes. Since the size distribution of NPs is fixed and the number as well as alignment of the molecules encapsulated within them remain unaffected (which is highly dependent on the size of NPs), we do not expect any interconversion of type I to type II molecular arrangement over time in the absence of any external perturbation. Sequential spectral measurements did not show any difference, as expected. After getting a clear solution, the samples are kept for stabilization over a few minutes; once the large dye particles outside the micellar cavity settle down, the clear solution from the top of the vial is used for further measurements. The aim of this work is to compare the effect of confinement on SF dynamics of TIPS-Pn in bulk and within NPs. Therefore, to compare the particles with bulk $CHCl_3$, the same amount of stock solution of TIPS-Pn is added into 2 ml of $CHCl_3$ and used for further measurements. The concentrations of TIPS-Pn in bulk $CHCl_3$, TX-100, CTAB, and SDS NPs are observed $\sim 1.8 \times 10^4 M$, $1.1 \times 10^4 M$, $0.65 \times 10^4 M$ and $0.45 \times 10^4 M$, respectively. The size of these micellar nanostructures with and without TIPS-Pn sample encapsulation is measured using a dynamic light scattering (DLS) spectrometer (Zetasizer, Nanoseries, Malvern Instruments). Further, the shape of these nanostructures is confirmed by high-resolution transmission electron microscopy (HR-TEM, JEMF200, JEOL) images which are taken after drop-casting the sample on the carbon-coated copper TEM grids (Agar Scientific) after desiccating over a few days.

Steady-state Spectral Measurements

The absorption spectra are collected in a UV-Vis spectrophotometer (Cary 5000 UV-Vis-NIR, Agilent Technologies) over a wide range of 350 nm to 900 nm and the fluorescence spectra are recorded in a steady-state fluorimeter (Cary Eclipse, Agilent Technologies) in the range of 650 nm to 900 nm after fixing the excitation at $\sim$635 nm.

Time-resolved Fluorescence Measurements

A laser diode (FWHM $<$200 ps) of 635 nm wavelength is used to excite TIPS-Pn inside NPs as well as in bulk $CHCl_3$ and the fluorescence lifetime is recorded in a time-correlated single-photon counting (Deltaflux, Horiba Scientific) spectrometer. The of instrument response function (IRF) is deconvoluted from the fluorescent data is done using scatter from a $\sim$0.1% colloidal solution (Ludox, Sigma-Aldrich). The lifetime traces are collected at the magic angle (54.7°) whereas anisotropy traces are collected at 0° and 90° polarization by fixing the peak preset as well as peak difference at 10,000 counts. The lifetime and anisotropy decays are fitted using DAS 6 analysis software. A detailed discussion on analysis of fluorescence lifetime and time-resolved anisotropy is provided in Supporting Information (hereafter, SI) section SI–III.

Transient Absorption (TA)

A broadband femtosecond transient absorption spectrometer (TAS, Newport) is used for ultrafast relaxation dynamics, the details of

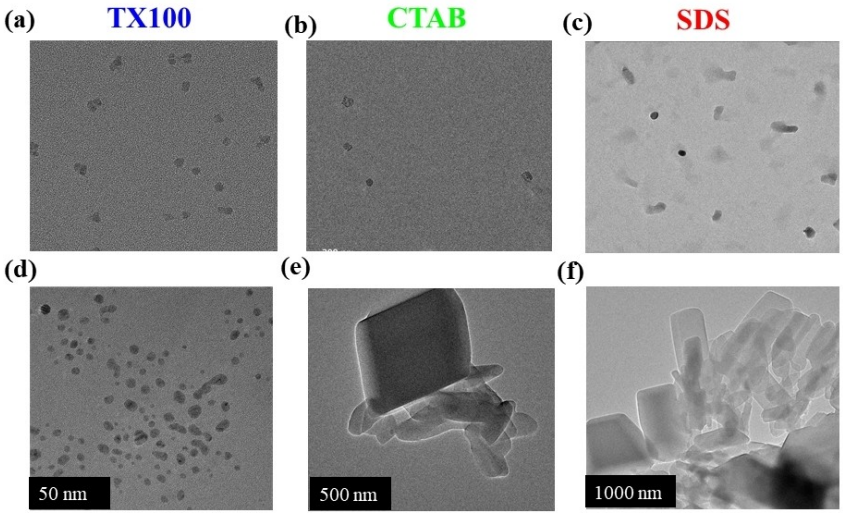

Figure 1. HR-TEM images of TX-100 (left), CTAB (middle), and SDS (right panel) micellar NPs without (a, b, c) and with (d, e, f) TIPS-Pn dye encapsulation, respectively at different scales.

which may be found elsewhere.[51,52] In brief, an excitation laser pulse centered at 640 nm with pulse-width ~30 fs is generated by a commercial non-collinear optical parametric amplifier (Topas White, Light conversion), seeded by a ~55 fs laser pulse centered on 800 nm from a Ti: Sapphire regenerative amplifier (Libra, Coherent). Part of the 800 nm laser pulse is focused on a CaF_2 crystal to generate a broadband white light probe pulse. The TA data are collected at pump magic angle (54.7°) with respect to the vertically polarized probe to negate anisotropic effects of the sample. The pump and probe power at sample position are maintained ~130 μW and 5 μW, respectively.

Details of pulse characterization and measurement of beam profiles may be found in sections SI-IV and SI-V, respectively. The data is analysed using open-source global analysis software (Glotaran, version 1.5.1) by assuming a three-state kinetic model (discussed later) for all the samples, and the figures are plotted using Matlab programming (Matlab2019a, MathWorks).

Results and Discussion

Since no significant change is observed with an increase in concentration 200/400/600/800/1000 μL of TIPS-Pn chromophores inside NPs, the dynamics is analysed for 200 μL in 2 ml surfactant solution as well as in bulk $CHCl_3$ throughout the experiment.

NP Size Distribution

The hydrophobicity of TIPS-Pn renders the chromophores stay inside micellar structures interacting with hydrocarbon chain of surfactants or in the Stern layer. The size and shape of different micellar structures encapsulated with TIPS-Pn are characterized using DLS and HR-TEM images. The average size of TX-100 NPs is observed ~6 nm which significantly increases up to ~120 nm for CTAB and ~500 nm for anionic SDS, with a large size distribution. After dye insertion, the shape of NPs changes significantly in case of CTAB and SDS, as shown in Figure S1, which may be due to aggregation of TIPS-Pn in the Stern layer of larger micellar nanostructures. The TEM images show spherical NPs for all surfactants without dye; however, after TIPS-Pn encapsulation, TX-100 shows no change in the shape whereas CTAB and SDS show rod-shaped NPs as shown in Figure 1.

Steady-state Studies

As shown in Figure 2, the absorption spectra of TIPS-Pn in $CHCl_3$ (monomer) shows $S_1 \leftarrow S_0$ transition at 642 nm and $S_2 \leftarrow S_0$

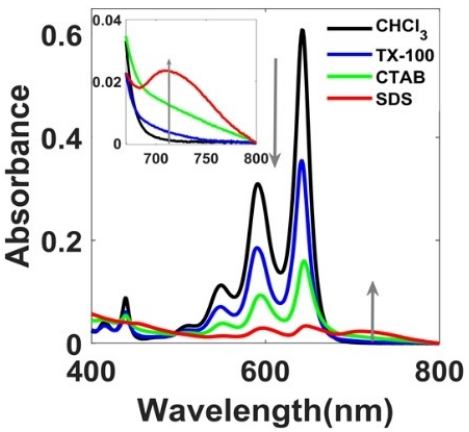

Figure 2. Plots for absorption spectra of TIPS-Pn in bulk $CHCl_3$ (black) and in TX-100 (blue), CTAB (green), SDS (red) micellar NPs. There are two conversion points, in which the 680 nm one represents the evolution of type I to type II coupling. Inset shows the evolution of type II arrangement of chromophores with an increase in size of NPs.

transition at 439 nm; the $S_1 \leftarrow S_0$ transition has shown three prominent vibrational manifolds corresponding to $0 \leftarrow 0$, $1 \leftarrow 0$, and $2 \leftarrow 0$ transitions at 642 nm, 591 nm, and 549 nm, respectively. A baseline correction for stead-state spectra of neat NP solutions is perfomed for all the samples; however, after dye encapsulation, more scattering is observed in larger-sized NPs which may be due to slight structural changes and hence the baseline cannot be corrected in the steady-state spectra. This, however, does not affect the time-resolved measurements. The $S_1 \leftarrow S_0$ transition of two types of distinct populations type I and type II are observed at 642 nm and 710 nm, respectively. 680 nm and 495 nm represent the conversion points of the oscillator strengths between S_1 and S_2 states and type I and type II populations, respectively. Absorption band at 710 nm is observed predominantly in NPs which increases significantly with an increase in size. This clearly indicates that in the present study, the interconversion of type I to type II molecular arrangement within NPs is highly dependent on the size of nanocavity, or in other words on the number of encapsulated chromophores (which is independent of time). However, in previous studies similar interconversion has been observed without any nanoconfinement for the time dependent morphological evolution of type II NPs.[34–36] Moreover, the absorption peaks show broadening with a slight redshift and decrease in the ratios of $0 \leftarrow 0$ to $1 \leftarrow 0$, and $2 \leftarrow 0$ peak heights, inside the micellar NPs of neutral, cationic, and anionic surfactants. In case of TX-100, the absorption spectra show no significant change from monomer which indicates the presence of weakly interacting chromophores inside NP as smaller size of nanocavity allows only a few molecules to encapsulate. However, in case of CTAB and SDS NPs, the $S_1 \leftarrow S_0$ transition shifts significantly red at 644 nm and 646 nm, respectively, reflecting the strength of coupling between chromophores is enhanced with an increase in size of nanoparticle whereas no shift is observed for $S_2 \leftarrow S_0$ transition as shown in Figure S2 (a).

Contrary to absorption, fluorescence spectra show unusual behaviour; fluorescence intensity of TIPS-Pn increases inside TX-100 whereas decreases in CTAB and SDS NPs. In highly concentrated solution of TIPS-Pn in $CHCl_3$, collision-induced (dynamic) quenching results in a slight decrease in fluorescence intensity which is most likely absent within smaller-sized TX-100 NP due to increased confinement leading to restricted diffusion and, thereby, less collisions. However, as the size of particle increases in case of CTAB and SDS, the intensity decreases due to strong coupling between chromophores, leading to (static) quenching of fluorescence. Moreover, no significant spectral shift is observed but the intensity of $1 \leftarrow 0$ band changes as shown in Figure S2 (b) which may be due to different interactions of TIPS-Pn with NPs. Since inside micellar nanostructures the chromophore accommodates the hydrophobic region, non-interaction is expected from the ionic/neutral headgroups of surfactants. Hence, the enhancement or reduction in fluorescence intensities of TIPS-Pn within NPs is highly dependent on the size and flexibility of NPs which ultimately control the relative extent of type I and II arrangements as well as the (dynamic and static) quenching within them. However, as discussed later, the enhanced fluorescence in TX-100 may also be contributed by enhanced singlet population; therefore, the increase/decrease in fluorescence may not be truly correlated with SF efficiency.

Time-resolved Fluorescence

The lifetime of TIPS-Pn in $CHCl_3$ is fitted with a single exponential and with a bi-exponential in TX-100 and a tri-exponential in CTAB and SDS nanostructures, respectively (see the SI-III for a detailed discussion about time-resolved fluorescence measurements), as shown in Figure S3 (a). A comparison of lifetime data is tabulated in Table S1 in SI. The lifetime of coupled chromophores can increase or decrease depending upon the efficiency of energy migration or quenching due to aggregation.[53,54] The longest lifetime component of monomer is observed ~11.2 ns in $CHCl_3$, whereas in TX-100 NPs two components are observed ~4.8 ns and 18 ns which may be due to presence of two different types of populations. The lifetime decays show three components of ~0.15 ns, 2.8 ns &11.8 ns in case of CTAB, and ~0.17 ns, 3.8 ns &18.3 ns in case of SDS NPs. The initial <300 ps component may be observed due to singlet excitonic energy transfer within strongly coupled chromophores (which cannot be resolved using TCSPC). The rest two components are due to relaxation of two distinct populations similar as TX-100. Neither the longest component nor the average lifetime follows a regular trend (as evident from Table S1); therefore, like steady-state fluorescence, fluorescence lifetime may not be truly correlated with SF efficiency.

To further explore the rotational dynamics of these NPs, as well as the location of the dye within them,[55] time-resolved anisotropy measurements are carried out. The anisotropy decays of TIPS-Pn in $CHCl_3$ are fitted with a single exponential whereas in TX-100, CTAB, and SDS NPs with a bi-exponential function as shown in Figure S3 (b). The anisotropy decay time constants are tabulated in Table S2 in SI. Recently, it was shown that local medium (solvent) can change the mechanism of fluorescence depolarization from rotational diffusion to energy transfer by restricting the motion of chromophores and their aggregates.[53,54] A discussion on the assignment of anisotropy time constants to different mechanisms of fluorescence depolarization is provided in SI-III. In case of TIPS-Pn in $CHCl_3$, the rotational time is observed around 0.33 ns which indicates fast rotation of monomer. However, the NPs show one sub-nanosecond component (<1 ns) and another nanosecond component (>10 ns). The sub-nanosecond component corresponds to the singlet exciton migration within type I or type I to type II molecular arrangement and the longer nanosecond component may be due to singlet exciton trap within type II arrangement of chromophores along with slow rotation of NPs.[36] It is noteworthy to mention here that the proximity effect of interface leading to slow solvation dynamics (due to restricted motion of solvent molecules present on the interface as well as in the core region) is observed for micelles up to a certain size beyond which the dynamics is similar to that exhibited by bulk solvent.[55] In the present study, atleast the site of the confinement is much larger and the chromophores preferentially

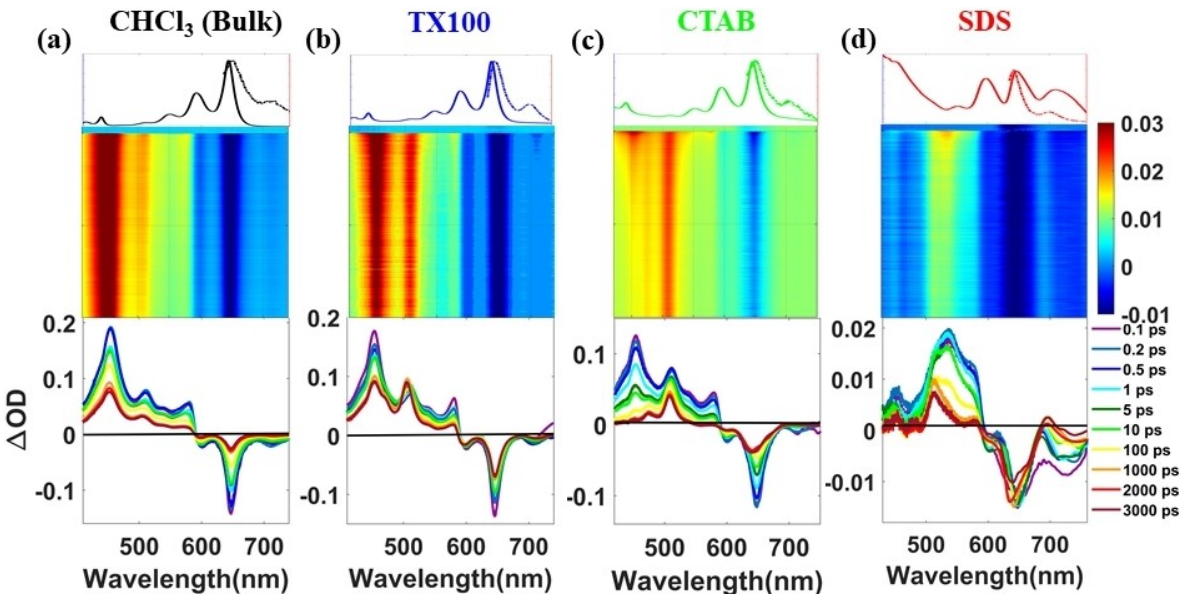

Figure 3. Plots for steady-state spectra (solid line corresponds to absorption, dashed to emission) along with the transient absorption heat map and spectral traces at various probe delays of TIPS-Pn in $CHCl_3$ (panel (a)), TX-100 (panel (b)), CTAB (panel (c)), and SDS (panel (d)).

accommodate the hydrophobic interfacial region which facilitate the interchromophoric coupling with an increase in size of nanocavity which is distinct from bulk.

Transient Absorption

To explore the sub-picosecond dynamics, transient absorption (TA) studies are performed. The pump pulse centered on 640 nm launches the population to the S_1 state of TIPS-Pn and the time-delayed probe pulse further interrogates this change. As shown in Figure 3, from 410 nm to 590 nm, a broad photoinduced absorption band is observed in all the samples with a variation on spectral shape; this indicates the presence of $S_n \leftarrow S_1$ transition at 410–490 nm region and $T_n \leftarrow T_1$ transition at 490–550 nm region.[14,35,36] A broad ground state bleach signal $S_1 \leftarrow S_0$ is observed in the region of 590 nm to 750 nm (corresponding to the absorption spectra of samples). In case of $CHCl_3$, the band ranging from 490 nm to 530 nm shows slight growth within <300 fs whereas in case of TX-100, CTAB, and SDS NPs the band exhibits a slower growth within <10 ps time scales; this clearly indicates that in case of NPs there is a significant generation of triplets from SF as compared to bulk solution. As the size of NP increases, the interconversion of type I to type II arrangements increase due to strong coupling between large numbers of chromophores. This shows a decrease in intensity of the band observed in the range of 410 nm to 480 nm, shown in Figure 4, which is most likely due to formation of singlet exciton trap within strongly coupled chromophores (with a concomitant decrease in photoinduced absorption from singlet). This singlet spectral feature reveals strong-coupling induced changes with an increase in size of NPs which were not explored in the previous report.[36] Moreover, if there is a (static) shift in electronic energy levels of type-I arrangement of TIPS-Pn due to confinement, for example, within SDS where it is more prominent, the absorption peaks should have been associated a larger shift which is not observed here (only ~4 nm red-shift is observed). However, type-II arrangement of TIPS-Pn shows significant redshift (~70 nm from type-I) in absorption spectra in SDS NPs which cannot be result of energy level fluctuations of type I..

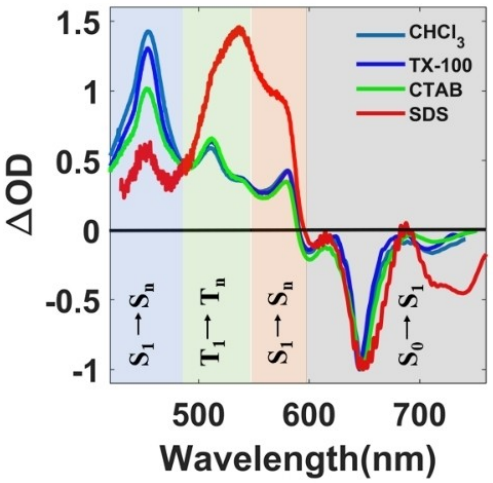

Figure 4. Plot of spectral traces of TIPS-Pn in bulk $CHCl_3$ (black) and TX-100 (blue), CTAB (green), SDS (red) micellar NPs at 100 fs probe delay, depicting various possible transitions.

To further confirm this, we consider a three-state kinetic model for SF. Since the formation of a geminate triplet (electronically coupled triplet pairs or 'correlated triplets') is very fast (~100 fs),[15] and lies at the limit of our experimental

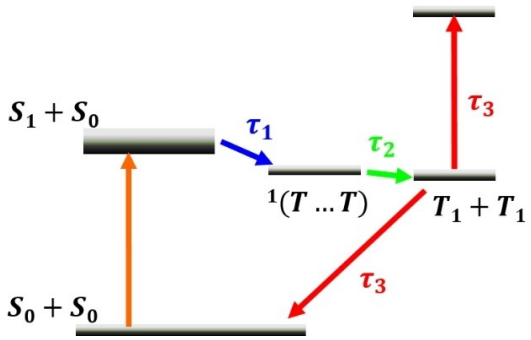

Figure 5. Proposed kinetic model for SF depicting the triplet exciton generation via geminate triplet pair, induced by a 640 nm pump pulse.

Table 1. The time constants obtained from global analysis.

Sample	τ_1*(ps)*	τ_2*(ps)*	τ_3*(ps)*
$CHCl_3$	5.0 ± 0.05	119 ± 3	1130 ± 41
TX100	1.34 ± 0.013	24.3 ± 0.2	1101 ± 16
CTAB	2.36 ± 0.009	24.4 ± 0.1	1194 ± 18
SDS	2.42 ± 0.04	39.0 ± 0.58	2732 ± 301

time resolution, it could not be captured. As shown in Figure 5, we assume that the singlet state undergoes SF via generation of a correlated triplet pair $(^1T...T)$ with a time constant of τ_1 which eventually get spatially separated to generate two independent triplet excitons $(T_1 + T_1)$ (mediated by diffusion) with a timescale τ_2;finally, the triplet excitons can decay or/and undergo annihilation (due to triplet-triplet collisions) with a time constant τ_3. Note that the kinetic model proposed in this article is highly inspired by the already tested models for SF in solids, solution, and aqueous suspensions of TIPS-pentacene nanoparticles.[14,15,36,37,40] Since, inside micellar nanostructures, we observed similar spectral features which only vary in intensities (most likely due to non-radiative relaxation which is highly dependent on size), indicating the participation of the same vibronic states. For SDS sample, the pump scattering (at 640 nm) is observed significantly owing to a larger size of the NP, which may cause spectral distortion in GSB signal. However, global analysis of pump probe data takes care of such scattering residual; therefore, no contribution from artifacts is expected in kinetic decay parameters. Moreover, the chromophore accommodates the hydrophobic region (as evident from linear spectrum and further supported by time-resolved anisotropy studies), no interference is expected from the ionic/neutral head-groups of surfactants that face the aqueous phase. In other words,in micelles, the charged head groups face outward (to the bulk aqueous phase) whereas the TIPS-Pn molecules are contained within the hydrophobic cavities which provide pretty much similar environment irrespective of the nature of charge of the head groups. Using global analysis with these three kinetic parameters, we obtain evolution-associated spectra and population dynamics, as shown in Figure 6 while the fitting parameters are tabulated in Table 1. We observe that in $CHCl_3$ the SF and the formation of triplet pair show time

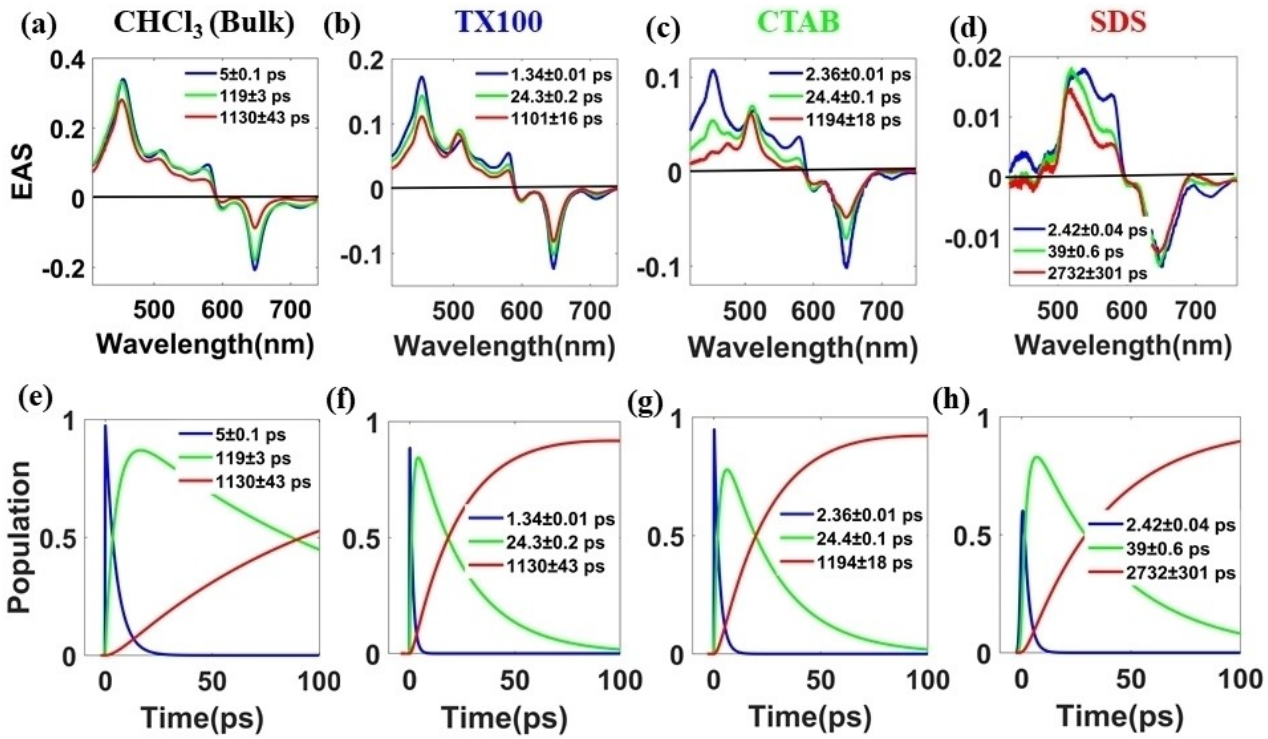

Figure 6. Plots of evolution associated decay spectra and population kinetics of TIPS-Pn in $CHCl_3$ (a & e), TX-100 (b & f), CTAB (c & g), and SDS (d & h) nanostructures, respectively.

constants of ~5 ps and ~119 ps, respectively, which are slower compared to NPs. In case of TX-100, the SF time constant is observed at ~1.34 ps which becomes slightly slower in case of CTAB (2.36 ps) and SDS (2.42 ps) NPs; this is on the order of the timescale ~2 ps is observed for TIPS-Pn NP suspension in previous reports.[35,36] Note that, one would expect the coupling strength to increase with decreasing NP size due to enhanced spatial confinement. However, as already mentioned, the coupling strength is highly dependent on specific packing of molecules within NPs which depends on the size as well as shape of the NPs. Smaller NPs (TX-100) favour type I linear arrangement which is responsible for weak coupling. On the other hand, strong coupling needs some optimal space (within the nanocavity) such that the molecules can self-assemble the brickwork packing, as exhibited by CTAB and SDS NPs. It should be brought in mind that, like the size of the NPs, the shape of the NPs is also highly dependent on the concentration of surfactant (CMC) and intercalation arrangement of the chromophore, which is difficult to control for micellar cavities; therefore, individual contributions from shape and size of the NPs cannot be separated. Thus, strong coupling within larger NPs facilitates the formation of traps that cannot undergo SF due to less competitive with non-radiative relaxation, resulting in slow SF time scales. However, despite the non-SF nature of such traps, there is always residual SF contributed by type I arrangement since both type I (weakly-coupled) and type II (strongly-coupled) arrangements of TIPS-Pn are present inside the NPs. Contrary to our results, previous studies proposed that with an increase in the concentration of type II arrangements, the SF rate becomes rapid within spontaneously formed NPs of pentacene derivatives contatining different functional groups, with no reports on singlet exciton traps.[35] However, recently it was proposed that in case of TIPS-Pn, the singlet exciton traps are formed due to slow morphological evolution leading to distortions in NPs, which are absent in crystals.[36] In the present study, the type II arrangement of chromophores persists within micellar NPs which are not very rigid; such flexibility in the nanostructures can give rise to singlet excitonic traps which slow down the SF rate. The formation of independent triplets from correlated triplet pair (or vice versa) takes place with a time constant of ~24 ps in case of TX-100 and CTAB which is faster compared to SDS NPs taking place at ~39 ps timescale; this may be due to formation of type II arrangements of chromophores within larger nanocavities and responsible for singlet exciton trap. Similar kinetics on the order of few tens of picosecond was observed in case of amorphous and crystalline TIPS-Pn thin films.[37] In SF, the free triplet state generation is further assisted by a recombination process known as triplet-triplet annihilation (TTA), which results in a decrease in lifetime of triplet state which ultimately reduces the triplet exciton's harvest efficiency.[37–40] The longer component (>1 ns) observed in NPs can be due to the recombination of triplets predominantly by TTA[37,40] or/and recombination to ground state after excitonic migration within strongly coupled chromophores;[36] this exciton migration generally occurs within a few tens of nanoseconds which may be more accurately estimated by joining the data sets corresponding to different temporal ranges/steps (instead of using only the data ranging 0 to 100 ps recorded at 0.1 ps steps, as discussed here) to cover the entire time window of 4 ns (corresponding to the maximum range of the mechanical delay stage) and is presented in SI-VII.

Further Discussion

A detailed discussion on estimating concentrations of triplet and singlet excited states with corresponding SF yield is provided in SI-VI. Table S3 in SI indicates the presence of a higher SF yield of TIPS-Pn within TX-100 NP which decreases with an increase in size of the NPs. However, least is observed in bulk $CHCl_3$; these results nicely correlate with the rates of SF. It is interesting to note here that both the concentrations of excited singlet and triplet increase in TX-100 with respect to bulk ($CHCl_3$), as evident from Table S3. Therefore, the observed increase in fluorescence intensity and lifetime in TX-100 may be due to the enhanced excited singlet population.

Moreover, to quantify the excitonic coupling within aggregates, the oscillator strength redistribution of 0–0 and 0–1 bands in micellar NPs, can be monitored. In case of H-aggregates, the ratio of oscillator strength of 0–0 and 0–1 vibrational bands in absorption spectrum diminishes.[56] However, we observed a significant increase in this ratio for TIPS-Pn in CTAB (2.23) and SDS (4) NPs as compared to bulk $CHCl_3$ (1.96) and TX-100 NP (1.96), indicating formation of J-type aggregates.

Furthermore, sensitization measurements (to ascertain triplet state quenching) cannot be performed due to the aqueous nature of these micellar nanostructures; however, it was reported previously that the excitaed state absorption features at >500 ps are due to triplet state absorption of TIPS-Pn[14,20,36] in the same singlet bleach region which further confirms the spectral assignments.

As a final note, though there exists a distribution of sizes for the NPs, no overlap between these distributions is observed indicating distinct dynamics within each NP. Of course, such distributions would mean that there is inhomogeneity as well heterogeneity in the system which can only be well resolved using excitation frequency-dependent studies (as in, 2DES[57] not captured by pump-probe measurements presented here.

Conclusions

To summarize, the studies presented here show how the size of micellar nanocavity adjusts an intricate balance between short-range and long-range interactions among chromophores under confinement, thereby controlling the efficiency of SF. These findings are a crucial step forward in understanding ultrafast dynamics of SF to harness carrier multiplication and thereby enhancing light-harvesting efficiency for photovoltaic applications.

Supporting Information

Time-resolved fluorescence analysis, Pulse width, and pump-probe beam profiles measurements in transient absorption studies, Calculation for SF yields. Plots for DLS data, steady-state spectra, time traces for fluorescence lifetime, and anisotropy. Tables for fitting parameters of fluorescence lifetime, time-resolved fluorescence anisotropy using TCSPC, and SF yield.

Acknowledgements

This work is funded by SERB, DST (CRG/2021/003981) and IISER Mohali (start-up grant). YS, SC and AD thank IISER Mohali for graduate fellowship to YS and SC and postdoctoral fellowship to AY. The authors would like to acknowledge IISER Mohali for the central HR-TEM (JEM-F200, JEOL) facility. It is a pleasure to thank Dr. Santanu Kumar Pal for letting them use the dynamic light scattering (DLS) spectrometer and Dr. Subhabrata Maiti for letting them use the steady-state fluorimeter.

Conflict of Interest

The authors declare no conflict of interest.

Data Availability Statement

The data that support the findings of this study are available in the supplementary material of this article.

Keywords: singlet fission · nano-confinement · excitonic trapping · femtosecond transient absorption spectroscopy · fluorescence anisotropy

[1] M. Schwoerer, H. C. Wolf, *Organic Molecular Solids*, WILEY-VCH, Weinheim **2007**.
[2] M. Kasha, H. R. Rawls, M. A. El-Bayoumi, *Pure Appl. Chem.* **1960**, *11*, 371–392.
[3] M. Kasha, *Radiat. Res.* **1963**, *20*, 55–71.
[4] M. Kasha, *Molecular Excitons in Small Aggregates, In Spectroscopy of the Excited State* (Eds.: B. Di Bartolo, D. Pacheco, V. Goldberg) Springer, Boston, MA, **1976**, Vol. 12, pp 337–363.
[5] W. Shockley, H. J. Queisser, *J. Appl. Phys.* **1961**, *32*, 510–19.
[6] S. Singh, W. J. Jones, W. Siebrand, B. P. Stoicheff, W. G. Schneider, *J. Chem. Phys.* **1965**, *42*, 330.
[7] J. J. Burdett, A. M. Muller, D. Gosztola, C. J. Bardeen, *J. Chem. Phys.* **2010**, *133*, 144506.
[8] R. P. Groff, P. Avakian, R. E. Merrifield, *Phys. Rev. B.* **1970**, *1*, 815.
[9] N. Geacintov, M. Pope, F. Vogel, *Phys. Rev. Lett.* **1969**, *22*, 593.
[10] M. Pope, C. E. Swenberg, *Electronic Processes in Organic Crystals and Polymers*, 2nd ed., Oxford University Press: New York, **1999**.
[11] G. B. Piland, C. J. Bardeen, *J. Phys. Chem. Lett.* **2015**, *6*, 1841–1846.
[12] E. A. Margulies, Y. L. Wu, P. Gawel, S. A. Miller, L. E. Shoer, R. D. Schaller, F. Diederich, M. R. Wasielewski, *Angew. Chem. Int. Ed.* **2015**, *54*, 8679–8683; *Angew. Chem.* **2015**, *127*, 8803–8807.
[13] A. A. Bakulin, S. E. Morgan, T. B. Kehoe, M. W. B. Wilson, A. W. Chin, D. Zigmantas, D. Egorova, A. Rao, *Nat. Chem.* **2015**, *8*, 16.
[14] B. J. Walker, A. J. Musser, D. Beljonne, R. H. Friend, *Nat. Chem.* **2013**, *5*, 1019.
[15] R. D. Pensack, E. E. Ostroumov, A. J. Tilley, S. Mazza, C. Grieco, K. J. Thorley, J. B. Asbury, D. S. Seferos, J. E. Anthony, G. D. Scholes, *J. Phys. Chem. Lett.* **2016**, *7*, 2370–2375.
[16] C. Schierl, A. Niazov-Elkan, L. J. Shimon, Y. Feldman, B. Rybtchinski, D. M. Guldi, *Nanoscale.* **2018**, *10*, 20147–20154.
[17] A. K. Le, J. A. Bender, S. T. Roberts, *J. Phys. Chem. Lett.* **2016**, *7*, 4922–4928.
[18] S. W. Eaton, L. E. Shoer, S. D. Karlen, S. M. Dyar, E. A. Margulies, B. S. Veldkamp, C. Ramanan, D. A. Hartzler, S. Savikhin, T. J. Marks, M. R. Wasielewski, *J. Am. Chem. Soc.* **2013**, *135*, 14701–14712.
[19] R. J. Dillon, G. B. Piland, C. J. Bardeen, *J. Am. Chem. Soc.* **2013**, *135*, 17278–17281.
[20] A. J. Musser, M. Maiuri, D. Brida, G. Cerullo, R. H. Friend, J. Clark, *J. Am. Chem. Soc.* **2015**, *137*, 5130–5139.
[21] C. Wang, M. J. Tauber, *J. Am. Chem. Soc.* **2010**, *132*, 13988–13991.
[22] J. N. Schrauben, J. L. Ryerson, J. Michl, J. C. Johnson, *J. Am. Chem. Soc.* **2014**, *136*, 7363–7373.
[23] J. C. Johnson, A. J. Nozik, J. Michl, *J. Am. Chem. Soc.* **2010**, *132*, 16302–16303.
[24] A. Rao, M. W. B. Wilson, J. M. Hodgkiss, S. A. Seifried, H. Bässler, R. H. Friend, *J. Am. Chem. Soc.* **2010**, *132*, 12698–12703.
[25] A. Rao, M. W. B. Wilson, S. A. Seifried, R. D. Pietro, R. H. Friend, *Phys. Rev. B.* **2011**, *84*, 195411.
[26] M. W. B. Wilson, A. Rao, B. Ehrler, R. H. Friend, *Acc. Chem. Res.* **2013**, *46*, 1330–1338.
[27] A. Kundu, J. Dasgupta, *J. Phys. Chem. Lett.* **2021**, *12*, 1468–1474.
[28] A. A. Bakulin, S. E. Morgan, T. B. Kehoe, M. W. B. Wilson, A. W. Chin, D. Zigmantas, D. Egorova, A. Rao, *Nat. Chem.* **2016**, *8*, 16–23.
[29] M. R. Wasielewski, *Acc. Chem. Res.* **2009**, *42*, 1910–1921.
[30] E. C. Greyson, J.-V. Weis, J. Michl, M. A. Ratner, *J. Phys. Chem. B.* **2010**, *114*, 14168–14177.
[31] W.-L. Chan, M. Ligges, X.-Y. Zhu, *Nat. Chem.* **2012**, *4*, 840–845.
[32] A. M. Alvertis, S. Lukman, T. J. H. Hele, E. G. Fuemmeler, J. Feng, J. Wu, N. C. Greenham, A. W. Chin, A. J. Musser, *J. Am. Chem. Soc.* **2019**, *141*, 17558–17570.
[33] G. Tao, *J. Phys. Chem. C.* **2019**, *123*, 29571–29579.
[34] C. B. Dover, J. K. Gallaher, L. Frazer, P. C. Tapping, A. J. Petty, M. J. Crossley, J. E. Anthony, T. W. Kee, T. W. Schmidt, *Nat. Chem.* **2018**, *10*, 305–310.
[35] R. D. Pensack, A. J. Tilley, S. R. Parkin, T. S. Lee, M. M. Payne, D. Gao, A. A. Jahnke, D. Oblinsky, P.-F. Li, J. E. Anthony, D. S. Seferos, G. D. Scholes, *J. Am. Chem. Soc.* **2015**, *137*, 6790–6803.
[36] M. J. Y. Tayebjee, K. N. Schwarz, R. W. MacQueen, M. Dvořák, A. W. C. Lam, K. P. Ghiggino, D. R. McCamey, T. W. Schmidt, G. J. Conibeer, *J. Phys. Chem. C.* **2016**, *120*, 157–165.
[37] K. T. Munson, J. Gan, C. Grieco, G. S. Doucette, J. E. Anthony, J. B. Asbury, *J. Phys. Chem. C.* **2020**, *124*, 23567–23578.
[38] A. D. Poletayev, J. Clark, M. W. Wilson, A. Rao, Y. Makino, S. Hotta, R. H. Friend, *Adv. Mater.* **2014**, *26*, 919–924.
[39] J. D. A. Lin, O. V. Mikhnenko, J. Chen, Z. Masri, A. Ruseckas, A. Mikhailovsky, R. P. Raab, J. Liu, P. W. M. Blom, P. M. A. Loi, *Mater. Horiz.* **2014**, *1*, 280–285.
[40] C. Grieco, G. S. Doucette, R. D. Pensack, M. Payne, A. Rimshaw, G. D. Scholes, J. E. Anthony, J. B. Asbury, *J. Am. Chem. Soc.* **2016**, *138*, 16069–16080.
[41] S. T. Roberts, R. E. McAnally, J. N. Mastron, D. H. Webber, M. T. Whited, R. L. Brutchey, M. E. Thompson, S. E. Bradforth, *J. Am. Chem. Soc.* **2012**, *134*, 6388–6400.
[42] N. Renaud, P. A. Sherratt, M. A. Ratner, *J. Phys. Chem. Lett.* **2013**, *4*, 1065–1069.
[43] W. Mou, S. Hattori, P. Rajak, F. Shimojo, A. Nakano, *Appl. Phys. Lett.* **2013**, *102*, 173301.
[44] L. Wang, Y. Olivier, O. V. Prezhdo, D. Beljonne, *J. Phys. Chem. Lett.* **2014**, *5*, 3345–3353.
[45] S. R. Yost, J. Lee, M. W. B. Wilson, T. Wu, D. P. McMahon, R. R. Parkhurst, N. J. Thompson, D. N. Congreve, A. Rao, K. Johnson, M. Y. Sfeir, M. G. Bawendi, T. M. Swager, R. H. Friend, M. A. Baldo, T. A. Van Voorhis, *Nat. Chem.* **2014**, *6*, 492–497.
[46] C. Sutton, N. R. Tummala, D. Beljonne, J.-L. Brédas, *Chem. Mater.* **2017**, *29*, 2777–2787.
[47] J. E. Anthony, J. S. Brooks, D. L. Eaton, S. R. Parkin, *J. Am. Chem. Soc.* **2001**, *123*, 9482–9483.
[48] A. N. Stuart, P. C. Tapping, E. Schrefl, D. M. Huang, T. W. Kee, *J. Phys. Chem. C.* **2019**, *123*, 5813–5825.

[49] Y. Silori, A. Yadav, S. Chawla, A. K. De, in *Proceedings of the International Conference on Ultrafast Phenomena 2022*, OSA Technical Digest (Optica Publishing Group, **2022**), In press.
[50] J. Zirzlmeiera, D. Lehnherrb, P. B. Cotoc, E. T. Chernickd, R. Casillasa, B. S. Basela, M. Thossc, R. R. Tykwinskid, D. M. Guldi, *Proc. Natl. Acad. Sci. USA* **2015**, *112* (17) 5325–5330.
[51] Y. Silori, S. Chawla, A. K. De, *ChemPhysChem.* **2020**, *21*, 1908–1917.
[52] A. Kalaiselvan, S. Dhamija, C. Aswathi, A. K. De, S. Gokulnath, *Chem. Commun.* **2021**, *57*, 11485–11488.
[53] Y. Silori, A. K. De, *J. Photochem. Photobiol. A* **2019**, *377*, 198–206.
[54] Y. Silori, A. K. De, *J. Mol. Liq.* **2019**, *298*, 112093.
[55] Y. Silori, S. Dey, A. K. De, *Chem. Phys. Lett.* **2018**, *693*, 222–226.
[56] F. C. Spano, *Acc. Chem. Res.* **2010**, *43*, 429–439.
[57] Y. Silori, P. Seliya, A. K. De, *J. Phys. Chem. B.* **2020**, *124*, 6825–6834.

Manuscript received: June 28, 2022
Revised manuscript received: July 12, 2022
Accepted manuscript online: July 13, 2022
Version of record online: September 2, 2022